Original Article

Predicting peritumoral Glisson's sheath invasion of intrahepatic cholangiocarcinoma with preoperative CT imaging

Yingfan Mao[1#], Yong Zhu[2#], Yudong Qiu[3], Weiwei Kong[4], Liang Mao[3], Qun Zhou[1], Jun Chen[5], Jian He[1]

[1]Department of Radiology, Nanjing Drum Tower Hospital, the Affiliated Hospital of Nanjing University Medical School, Nanjing 210008, China; [2]Department of Radiology, Jiangsu Province Hospital of Traditional Chinese Medicine, the Affiliated Hospital of the Nanjing University of Chinese Medicine, Nanjing 210008, China; [3]Department of Hepatopancreatobiliary Surgery, [4]Department of Oncology, [5]Department of Pathology, Nanjing Drum Tower Hospital, the Affiliated Hospital of Nanjing University Medical School, Nanjing 210008, China

[#]These authors contributed equally to this work.

Correspondence to: Jian He, MD. Department of Radiology, Nanjing Drum Tower Hospital, the Affiliated Hospital of Nanjing University Medical School, No. 321 Zhongshan Road, Nanjing 210008, China. Email: hjxueren@126.com; Jun Chen, PhD. Department of Pathology, Nanjing Drum Tower Hospital, the Affiliated Hospital of Nanjing University Medical School, No. 321 Zhongshan Road, Nanjing 210008, China. Email: ichenjun@qq.com.

Background: To investigate the differences of clinicopathological characteristics and computed tomography (CT) features between intrahepatic cholangiocarcinomas (ICC) with and without peritumoral Glisson's sheath invasion (PGSI), and to construct a nomogram to predict PGSI of ICCs preoperatively.

Methods: The clinicopathological characteristics and CT features of 84 ICCs were retrospectively analyzed and compared between ICCs with (30/84, 35.7%) and without PGSI (54/84, 64.3%). Multivariate logistic regression analysis was used to identify preoperative independent predictors of PGSI in ICCs. A nomogram was constructed to predict PGSI preoperatively.

Results: ICCs with and without PGSI differed significantly in the presence of abdominal pain, serum carcinoembryonic antigen (CEA) and carbohydrate antigen 19-9 (CA19-9) levels, TNM and T stages, tumor location, intratumoral calcifications, intrahepatic bile duct dilatation, intrahepatic bile duct calculus, morphologic type and dynamic enhancement pattern on CT images (all $P<0.05$). Abdominal pain, serum CEA level, intrahepatic bile duct dilatation, and morphologic type were independent predictors of PGSI in ICCs. A nomogram based on those predictors was constructed to predict PGSI preoperatively with an area under the receiver operating characteristic (ROC) curve (AUC) of 0.908 ($P<0.001$).

Conclusions: Clinicopathological characteristics and CT features differed significantly between ICCs with and without PGSI. A nomogram including abdominal pain, serum CEA level, intrahepatic bile duct dilatation, and morphologic type could predict PGSI accurately.

Keywords: Intrahepatic bile ducts; cholangiocarcinoma; peritumoral Glisson's sheath; spiral computed tomography; nomogram

Submitted Oct 20, 2018. Accepted for publication Dec 04, 2018.
doi: 10.21037/qims.2018.12.11
View this article at: http://dx.doi.org/10.21037/qims.2018.12.11

Introduction

Intrahepatic cholangiocarcinoma (ICC) originates from the biliary epithelial cells of the secondary hepatic bile ducts and their branches. ICC is the second most common primary liver cancers after hepatocellular carcinoma (1,2), accounting for approximately 10% of all primary liver cancers (3). The incidence of ICC is increasing worldwide (4).

Glisson's sheath is a layer of fibrous connective tissue wrapping around the portal vein, hepatic artery, and bile duct. During the development of ICCs, tumor cells could

spread into the extrahepatic bile duct and lymph nodes through peritumoral Glisson's sheath (5). Hence, cancerous cells spreading along peritumoral Glisson's sheath has been described as a distinct way of metastasis in ICCs by World Health Organization (WHO) [2010] (6). Since peritumoral Glisson's sheath invasion (PGSI) reflects the invasion and migration capability of ICCs, it is essential to predict PGSI preoperatively to optimize treatment strategy and predict the prognosis of those patients.

Computed tomography (CT) is a commonly used and sophisticated technique for preoperative evaluation of ICC (7,8). Asayama *et al.* described in their article that the CT enhancement degree of mass-forming (MF) ICC on the late phase is a useful predictor of prognosis (9). Yamamoto *et al.* reported that a CT ratio (CT value of tumor/liver parenchyma in late arterial phase) less than 0.88 is a preoperatively measurable independent risk factor for lymph node metastasis in ICC (10). Based on those findings, we hypothesized that there might be some differences of CT features and clinicopathological characteristics between ICCs with and without PGSI, which has never been documented before.

So, this study aimed to investigate the differences of clinicopathological characteristics and CT features between ICCs with and without PGSI and to establish a nomogram for predicting preoperative PGSI in ICCs.

Methods

Patients

The retrospective study was approved by the local institutional review board, and the informed consent from patients was waived. A total of 175 patients with a clinical diagnosis of ICC were collected between November 2007 and July 2017. The inclusion criteria were: (I) with a postoperative pathological diagnosis of ICC according to 2010 World Health Organization classification criteria by postoperative specimens; (II) CT images within two weeks before treatment initiation; (III) with definite PGSI status confirmed by postoperative pathological results derived from specimens; (IV) without any systemic or local treatment before CT examination and surgery, for instance, radiofrequency ablation, transcatheter arterial chemoembolization, chemotherapy or radiotherapy. The exclusion criteria were: (I) perihilar cholangiocarcinoma invading the liver (n=9); (II) unclear CT images because of artifacts (n=3) or unclear tumor on CT images (n=2).

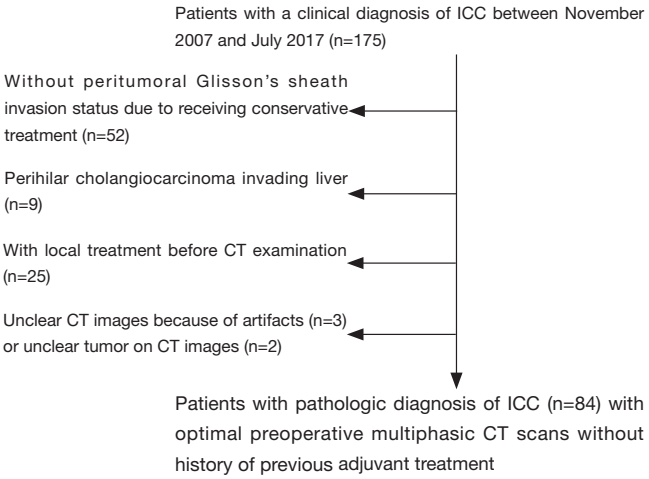

Figure 1 Flow-chart of inclusion and exclusion of this study.

Finally, 84 patients served as our study cohort, including 53 males and 31 females, with an average age of 59.3±10.3 years (range, 33–79 years). The flowchart of inclusion and exclusion in this study is shown in *Figure 1*.

Preoperative clinical data and postoperative pathological information of those patients were obtained from the electronic medical record system which is exhibited in *Table 1*.

CT examination

From right side diaphragm to the pubic symphysis, all patients underwent CT scanning on a multidetector spiral CT scanner (Lightspeed, VCT, or Discovery HD750, GE Healthcare, US) in the supine position. CT scan parameters were as follows: tube voltage 120 kVp, tube current 250–350 mA, collimating slice thickness 5 mm, reconstruction slice thickness 1.25 mm, slice interval 5 mm, rotation time 0.6 s, helical pitch 1.375, the field of view between 35 and 40 cm, matrix 512×512. A standard reconstruction algorithm was used. After unenhanced CT scan, A 1.2 mL/kg per body weight contrast agent (Omnipaque 350 mgI/mL, GE Healthcare, US) was injected into the patient's elbow vein using a power injector (Medrad tellant, Indianola, PA, US) at an injection rate of 3.0 mL/s, and then 40 mL of saline solution was injected at the same injection rate. The time to obtain the arterial phase, the portal venous phase, and the equilibrium phase image were 35 s, 70 s, and 3 min after the injection of the contrast agent, respectively. The mean interval between the CT scan and surgery was 8.3±4.2 days (range, 5–23 days).

Table 1 The clinicopathological characteristics of intrahepatic cholangiocarcinomas with (+) and without (–) PGSI

Characteristic	Total (n=84)	PGSI (+) (n=30)	PGSI (–) (n=54)	P value
Gender (male/female)	53/31	15/15	38/16	0.064
Age (years)	59.3±10.3 [33–79]	59.3±10.6 [33–76]	59.4±10.2 [34–79]	0.996
Chronic viral hepatitis (with/without)	54/30	16/14	38/16	0.118
Abdominal pain (with/without)	32/52	18/12	14/40	0.002
CEA (>/≤5 ng/mL)	21/63	15/15	6/48	<0.001
CA19-9 (>/≤37 U/mL)	51/33	21/9	23/31	0.016
AFP (>/≤10 ng/mL)	11/73	5/25	6/48	0.700
CA125 (>/≤35 U/mL)	16/68	7/23	9/45	0.456
Differentiation degree (well/well-moderate/moderate/moderate-poor/poor)	1/5/41/27/10	0/3/13/12/2	1/2/28/15/8	0.318
TNM stage (I/II/III/IV)	59/7/10/8	5/7/9/9	30/18/1/5	<0.001
T stage (T1/T2a/T2b/T3)	36/16/17/15	6/3/8/13	30/13/9/2	<0.001
N stage (Nx/N0/N1)	47/24/13	14/8/8	33/16/5	0.113

PGSI, peritumoral Glisson's sheath invasion; CEA, carcinoembryonic antigen; CA19-9, carbohydrate antigen 19-9; AFP, alpha-feto protein; CA125, cancer antigen 125; T and TNM stage determined based on the 7th edition of the American Joint Committee on Cancer (AJCC)/Union for International Cancer Control (UICC) staging system.

CT imaging interpretation

Two radiologists (M.Y.F. and Z.Y., with 3 and 7 years of experience in abdominal radiology, respectively) analyzed CT images independently without knowing the clinicopathological information of patients. In case of any discrepancy, the consensus was reached by discussions or consultations with a senior radiologist (H.J., with 12 years of experience in abdominal radiology). To avoid bias as far as possible, the most significant lesion was selected in 5 patients who have multiple lesions (2, 2, 2, 2, 15, respectively).

The criteria for assessing CT features of tumors were as follows: (I) Tumor number. Solitary or multiple. (II) Tumor location. Confined to the right lobe of the liver or not. (III) Tumor size. The maximum diameter of the tumor measured on axial CT image on the portal venous phase (in centimeters). (IV) Morphologic type. MF type and non-MF type according to its gross morphology on CT imaging (*Figure 2*). Non-MF type includes periductal-infiltrating (PI), intraductal-growing (IG) and MF&PI types (11,12). (V) Intratumoral calcifications. Dense foci on unenhanced CT images [CT value >100 Hounsfield units (HUs)] (13). (VI) Tumor necrotic or cystic components. Areas without obvious enhancement within the tumor on contrast-enhanced CT images. (VII) Intrahepatic bile duct dilatation. Dilated intrahepatic bile duct on contrast-enhanced CT images, whether local or diffuse, mild or severe (14). (VIII) Intrahepatic bile duct calculus. High-density nodular or patchy shadow within the dilated intrahepatic bile ducts on unenhanced CT scan (CT value >100 HU). (IX) Extrahepatic bile duct dilatation. A luminal diameter of common bile duct dilatation over 11 mm without cholecystectomy (15). (X) Satellite nodules. Daughter lesions around the larger main lesion. (XI) Adjacent liver contour. Smooth, bulging or retracted liver capsule.

Then, the axial CT image with a slice thickness of 1.25 mm showing the largest slice of the lesion was selected. A round or oval region of interest (ROI) was set in remarkably enhanced solid component of the lesion (mean area, 10.5±2.0 mm^2; range, 8.0–12.0 mm^2) to obtain the mean CT attenuation (in HU). The ROI was drawn as large as possible excluding visible vessels, necrosis or calcifications. A second round/oval ROI was placed in non-tumorous liver parenchyma in the same slice as large as possible (mean area, 4,967.2±607.3 mm^2; range, 4,000.0–5,500.0 mm^2) avoiding visible vessels to obtain the mean CT attenuation (in HU). The ROIs in the tumor and non-tumorous liver parenchyma were kept identical in the arterial, portal venous and equilibrium phases (*Figure 2*). CT values (HU) of the tumor in each phase were recorded

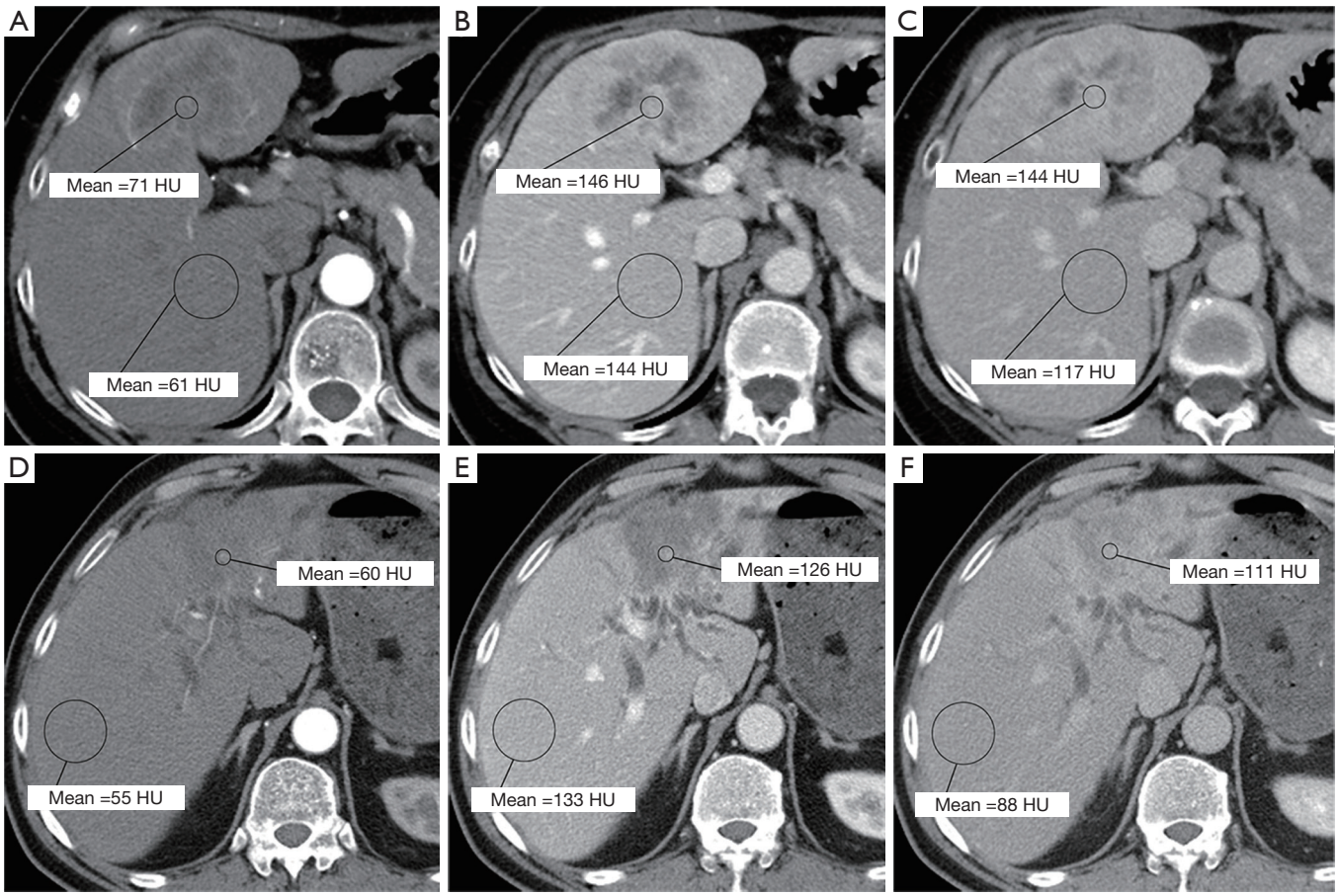

Figure 2 Axial CT images show a mass-forming (MF) type intrahepatic cholangiocarcinoma (ICC) in the arterial phase (A), portal venous phase (B) and equilibrium phase (C) in an 85-year-old woman. Axial CT images show a non-MF type ICC in the arterial phase (D), portal venous phase (E) and equilibrium phase (F) in an 83-year-old man. A region of interest (ROI) is placed in solid part of the lesion with remarkable enhancement avoiding visible vessels, necrosis or calcifications in each phase. A second ROI is placed in non-tumorous liver parenchyma in the same slice as large as possible avoiding visible vessels in each phase.

respectively. In each phase, tumor enhanced ratio =(CT value of tumor)/(CT value of normal liver). Each observer drew ROIs for three times to obtain the mean CT value. The result was the average of two radiologists.

According to our own experience and previous researches (4,16), There were three types of dynamic enhancement patterns of the tumor. (I) Progressive pattern: compared to the arterial phase, the degree and range of enhancement increased in portal venous or equilibrium period (CT value change ≥10 HU). (II) Persistent pattern: from the arterial phase to equilibrium phase, the degree and range of enhancement remained virtually unchanged (CT value change <10 HU). (III) Wash-in and wash-out pattern: the degree of improvement is naturally high in the arterial phase and decreased in the portal venous or equilibrium phase (CT value change ≥10 HU).

PGSI status

Postoperative specimens were placed in 10% formalin solution, fixed in a paraffin block, sliced and stained with hematoxylin-eosin. A pathologist (C.J., with 15 years of experience in liver pathology) who was blinded to clinical information and CT features of the patients observed the slices microscopically. PGSI was confirmed with the following four criteria (17): (I) cancer cells were found in the portal area around the tumor; (II) cancer cells infiltrated the fiber tissues of Glisson's sheath rather than microvessels in portal area; (III) the bile duct in portal area showed no atypia; (IV) there were normal hepatic tissues between

portal area and tumor.

Statistical analyses

Shapiro-Wilk test was performed to confirm the normality of all CT features in ICCs with and without PGSI. Quantitative data in normal distribution were expressed as mean ± standard deviation, and count data were represented as ratios. Differences of clinicopathological characteristics and CT features between ICCs with and without PGSI were tested by chi-square test for categorical variables, t-test or Mann–Whitney U test for continuous variables. Interobserver consistency of CT features was evaluated with Kappa test for categorical variables and with the intraclass correlation coefficient for continuous variables. Univariate analysis was used to screen out risk factors of PGSI in ICCs. Multivariate logistic regression analysis was performed on the significant factors (P<0.05) from univariate analysis using a Cox proportional hazards model to identify independent predictors of PGSI. The goodness of fit of the multivariate logistic regression model was tested by the Hosmer-Lemeshow test and a P value >0.05 stated that the model matches well. Receiver operating characteristic (ROC) analysis was performed to calculate the cut-off value. Next, there was recording based on the sensitivity, specificity, positive predictive value, negative predictive value, positive likelihood ratio, and negative likelihood ratio. A nomogram based on the prediction model was constructed to predict PGSI of ICCs preoperatively. Then, the specified score for each predictor based on the coefficients in the model was determined. SPSS version 18.0 (SPSS Inc., Chicago, IL, US) was used for all statistical analyses, and the parameters were considered statistically significant when the two-tailed P value was less than 0.05.

Results

Clinicopathological differences between ICCs with and without PGSI

There were 30 ICCs with PGSI (30/84, 35.7%) and 54 ICCs without PGSI (54/84, 64.3%). As shown in *Table 1*, ICC patients with PGSI presented with abdominal pain, increased serum CEA (>5 ng/mL) and CA19-9 levels (>37 U/mL) more often than ICCs without PGSI (60.0% *vs.* 25.9%, 50.0% *vs.* 11.1%, 70.0% *vs.* 42.6%, P=0.002, <0.001 and 0.016, respectively). ICCs with PGSI tend to be presented as higher TNM and T stage (both P<0.001).

CT features' differences between ICCs with and without PGSI

Interobserver consistency of CT features between the two radiologists was good with kappa values from 0.724 to 1 and intraclass correlation coefficients from 0.722 to 0.831. As shown in *Table 2*, ICCs with PGSI were confined to the right lobe of liver significantly less often than ICCs without PGSI (26.7% *vs.* 51.9%, P=0.025). ICCs with PGSI presented with intratumoral calcifications, intrahepatic bile duct dilatation and intrahepatic bile duct calculus more often than ICCs without PGSI (16.7% *vs.* 0%, 76.7% *vs.* 31.5%, 26.7% *vs.* 3.7%; P=0.009, <0.001, 0.006, respectively). ICCs with PGSI showed MF type significantly less often than ICCs without PGSI (60% *vs.* 88.9%, P=0.002). As shown in *Table 3*, the dynamic enhancement pattern differed significantly between ICCs with and without PGSI (P=0.041). ICCs with PGSI could show a persistent pattern (16.7%) but never wash-in and wash-out pattern (0%), while ICCs without PGSI showed persistent (5.6%) or wash-in and wash-out pattern (13.0%). Nevertheless, there were no significant differences of tumor CT value or enhanced tumor ratio between ICCs with and without PGSI on each phase (all P>0.05) (*Table 4*).

Logistic regression analysis and construction of a nomogram

As shown in *Table 5*, univariate analysis indicated seven variables as risk factors of PGSI in ICCs, including abdominal pain, serum CA19-9 level, serum CEA level, tumor location, morphologic type, intrahepatic bile duct dilatation, and intrahepatic bile duct calculus (all P<0.05). Multivariate logistic regression analysis identified abdominal pain, serum CEA level, intrahepatic bile duct dilatation and morphologic type as independent predictors of PGSI in ICCs (all P<0.05).

By imputing exact values of multiple variables into the multivariate logistic regression model, with an output larger than 0.427, we can predict PGSI of ICCs with a sensitivity of 0.786, a specificity of 0.800, an accuracy of 0.795, a positive predictive value of 0.690, a negative predictive value of 0.880, a positive likelihood ratio of 3.93, and a negative likelihood ratio of 0.268. The area under the ROC curve (AUC) was considered excellent (0.908; 95% confidence interval, 0.846–0.970) (*Figure 3*). With the aim of providing a practical tool for clinicians, a nomogram was constructed based on this model (*Figure 4*). Draw a vertical line and connect the value of each variable with the point score at the top of the diagram to

Table 2 CT features of intrahepatic cholangiocarcinomas with (+) and without (–) peritumoral Glisson's sheath invasion (PGSI)

CT feature	Total (n=84)	PGSI (+) (n=30)	PGSI (–) (n=54)	P value
Tumor number (solitary/multiple)	79/5	27/3	52/2	0.492
Tumor location (confined to right lobe/not)	36/48	8/22	28/26	0.025
Tumor size (cm)	5.5±2.4 (2.0–10.5)	5.7±2.3 (2.0–10.3)	5.5±2.5 (2.0–10.5)	0.741
Morphologic type (MF/non-MF)	66/18	18/12	48/6	0.002
Intratumoral calcifications (with/without)	5/79	5/25	0/54	0.009
Tumor necrotic or cystic components (with/without)	17/67	7/23	10/44	0.599
Intrahepatic bile duct dilatation (with/without)	40/44	23/7	17/37	<0.001
Intrahepatic bile duct calculus (with/without)	10/74	8/22	2/52	0.006
Extrahepatic bile duct dilatation (with/without)	15/69	7/23	8/46	0.329
Satellite nodules (with/without)	13/71	5/25	8/46	1.000
Liver contour (smooth/bulging/retraction)	39/10/35	12/5/13	27/5/22	0.520

MF, mass-forming.

Table 3 Dynamic enhancement pattern of intrahepatic cholangiocarcinomas with (+) and without (–) peritumoral Glisson's sheath invasion (PGSI) on CT images

Dynamic enhancement pattern	Total (n=84)	PGSI (+) (n=30)	PGSI (–) (n=54)
Progressive pattern	69 (82.1%)	25 (83.3%)	44 (81.5%)
Persistent pattern	8 (9.5%)	5 (16.7%)	3 (5.6%)
Wash-in and wash-out pattern	7 (8.3%)	0 (0%)	7 (13.0%)

P=0.041 with Chi-square test.

Table 4 CT indexes of intrahepatic cholangiocarcinoma with (+) and without (–) peritumoral Glisson's sheath invasion (PGSI)

CT index	PGSI (+) (n=30)	PGSI (–) (n=54)	P value
AP CT value of tumor	87.93±30.50	90.96±26.30	0.634
AP CT value of tumor/liver	1.30±0.42	1.38±0.36	0.351
PV CT value of tumor	119.27±29.63	128.15±39.57	0.287
PV CT value of tumor/liver	1.03±0.27	1.09±0.28	0.330
EP CT value of tumor	113.83±23.95	113.93±32.04	0.990
EP CT value of tumor /liver	1.19±0.35	1.19±0.25	0.955

AP, arterial phase; PV, portal venous phase; EP, equilibrium phase.

achieve the scores for each variable. Then add the scores of each variable to get the total point score, which is plotted along the "total points" line at the bottom of the nomogram. This line is projected to the probability of PGSI in ICC. Illustrations for the usage of this nomogram in predicting PGSI of two ICC patients are presented in *Figure 5A,B*. Pathological figures of PGSI status for the two ICC patients are shown in *Figure 5C,D*.

Discussion

In this study, the clinicopathological characteristics and CT

Table 5 Univariate and multivariate analysis of peritumoral Glisson's sheath invasion (PGSI) in intrahepatic cholangiocarcinoma patients

Variable	Univariate analysis P value	Multivariate analysis	
		Odds ratio (95% CI)	P value
Abdominal pain	0.003	6.802 (1.631–28.365)	0.008
CEA	<0.001	43.461 (5.904–319.940)	<0.001
CA19-9	0.022		
Tumor location	0.028		
Morphologic type	0.003	5.225 (1.105–24.704)	0.037
Intraumoral calcifications	0.999		
Intrahepatic bile duct dilatation	<0.001	13.976 (2.394–81.594)	0.003
Intrahepatic bile duct calculus	0.007		
Dynamic enhancement pattern	0.288		

CEA, carcinoembryonic antigen; CA19-9, carbohydrate antigen 19-9; CI, confidence interval.

features of 84 ICC patients were retrospectively analyzed, and many differences were detected between ICCs with and without PGSI, which has never been reported previously.

We found that ICC patients with PGSI presented with abdominal pain more often than those who had not. Moreover, ICCs with PGSI tend to be presented as higher TNM and T stage. Weber *et al.* reported that ICC patients with advanced stage usually presented with a wide array of symptoms including abdominal discomfort (18). Additionally, we found that ICCs with PGSI showed intrahepatic bile duct calculus more often than ICCs without PGSI. Hur *et al.* reported that abdominal pain appeared in all ICC patients with intrahepatic bile duct calculus (19). We speculated that intrahepatic bile duct calculus might be involved with abdominal pain in ICC patients with PGSI.

We found that ICCs with PGSI presented with increased serum CEA and CA19-9 levels significantly more often than ICCs without PGSI. It was reported that increased serum CEA and CA19-9 levels correlated with advanced stage, high recurrence rate and poor prognosis in ICC patients (20-22). Qin *et al.* reported that ICCs with lymph node metastasis, nerve infiltration or venous invasion presented with increased serum CEA and CA19-9 levels more often than those without (20). Based on those findings, we speculated that increased serum CEA and CA19-9 levels indicated a higher aggressiveness of ICCs.

We found that ICCs with PGSI presented as non-MF type significantly more often than ICCs without PGSI. Previous studies reported that in contrast to MF type, PI type ICCs tended to spread along the bile duct wall via the nerve and perineural tissue of Glisson's sheath toward the porta hepatis (23,24). Sandrine *et al.* reported that the MF&PI type ICCs was mostly coupled with portal vein invasion and lymph node involvement (25). Clinicopathological characteristics and biological behaviors of ICCs differed significantly among different macroscopic types (25).

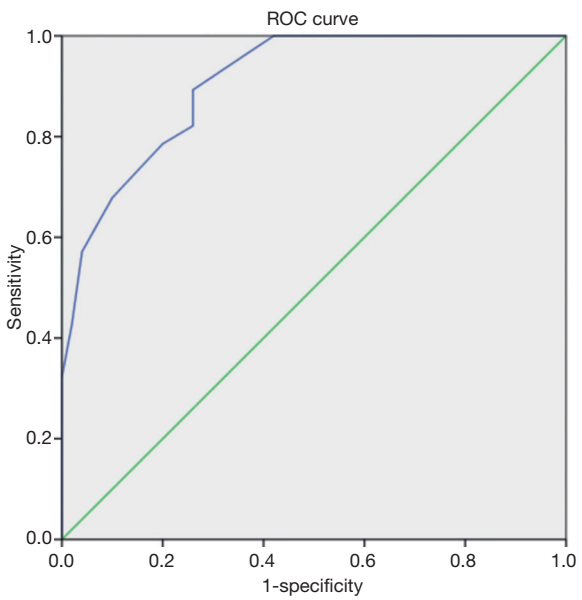

Figure 3 Receiver operating characteristic (ROC) curve of multivariate logistic analysis model in predicting peritumoral Glisson's sheath invasion of intrahepatic cholangiocarcinomas shows an area under the curve (AUC) of 0.908 (95% confidential interval, 0.846–0.970).

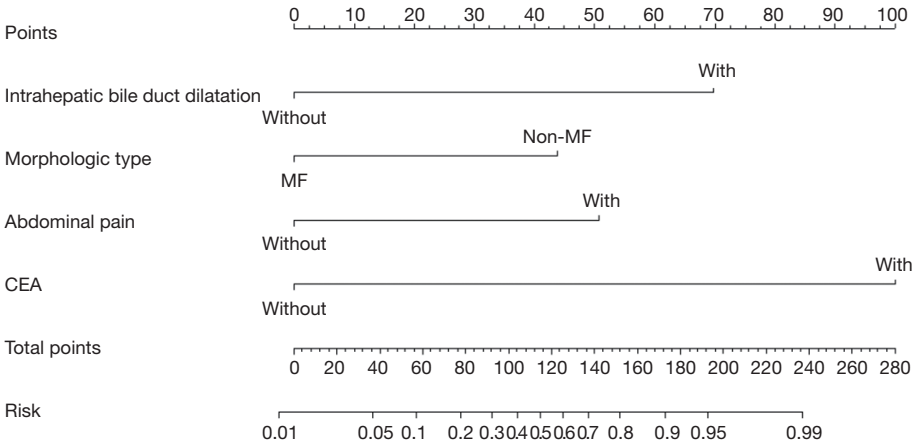

Figure 4 Nomogram represents the probability of peritumoral Glisson's sheath invasion of intrahepatic cholangiocarcinomas.

We found that ICCs with PGSI presented with a persistent pattern more often than those without, but presented with wash-in and wash-out pattern less often than those who had not. Histologically, the persistent pattern may be involved with the proportion and distribution of pathological components including adenocarcinoma, fibrosis and coagulation necrosis (26,27), while wash-in and wash-out pattern might be included with a more substantial proportion of survival tumor cells and differentiation degree of ICCs (28-30).

We found that ICCs with PGSI presented with intrahepatic bile duct dilatation more often than ICCs without PGSI. Previous studies reported an incidence of 41–52% for intrahepatic bile duct dilatation in ICCs (26,31), which played an essential role in the CT diagnosis of ICCs (31-33). In our study, the incidence of intrahepatic bile duct dilatation was 47.6% in ICCs, which accorded with previous studies. We suspected that ICCs with PGSI might infiltrate the bile duct or secrete mucin more often than ICCs without PGSI, leading to intrahepatic bile duct dilatation (12,26).

We found that there were no significant differences of tumor CT value or enhanced tumor ratio between ICCs with and without PGSI on each phase. Nevertheless, Asayama *et al.* and Yamamoto *et al.* suggested that CT enhancement degree was associated with perineural invasion and lymph node metastasis in mass-forming ICC (9,10), probably due to different study aim and samples from ours.

The preoperative predictors of PGSI in ICCs were identified by multivariate logistic regression analysis, including abdominal pain, serum CEA level, intrahepatic bile duct dilatation, and morphologic type. A nomogram based on those variables could predict PGSI of ICCs with an AUC of 0.908. We speculated that ICCs with PGSI often occur in proximal intrahepatic bile ducts, leading to bile duct stricture and distal bile duct dilatation. ICCs with PGSI behave more aggressively and efficiently invade surrounding structures, presenting at a more advanced stage with clinical symptoms such as abdominal pain. ICCs with PGSI might synthesize and secrete CEA and CA19-9 more than those without PGSI.

Nevertheless, the specific pathological foundation and underlying molecular mechanisms require more investigation. In our center, if preoperative assessment considers ICC to be present with PGSI, neoadjuvant therapy will be discussed. An accurate prediction of PGSI may optimize treatment planning and prognosis prediction in ICC patients, even without postoperative pathological information.

There were some limitations to this study. First, it was a single-center retrospective study, the sample size is relatively small, but this may pave the way for a large study. Second, selective bias was inevitable due to the study design, many patients at advanced stage losing the chance of surgery, who had to be excluded from the study. Third, the pathological foundation and molecular mechanisms of clinicopathological characteristics and CT features' differences between ICCs with and without PGSI required further investigation.

In conclusion, ICCs with and without PGSI were significantly different in tumor location and dynamic enhancement pattern on CT images. Abdominal pain, serum CEA level, intrahepatic bile duct dilatation, and morphologic type were independent predictors of PGSI in ICC patients. A nomogram based on those variables could predict PGSI of ICCs accurately, which characterized a

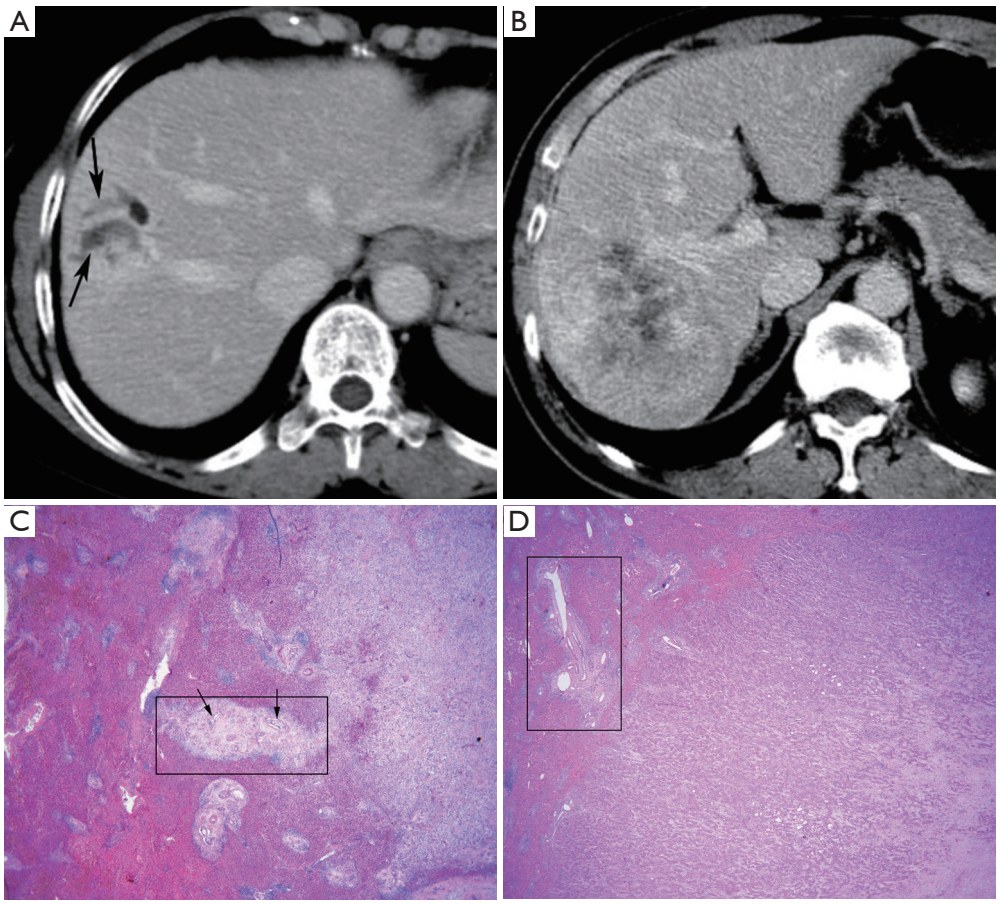

Figure 5 The usage of nomogram in predicting peritumoral Glisson's sheath invasion (PGSI) of two intrahepatic cholangiocarcinoma (ICC) patients and their pathological results. (A) A 57-year-old woman of ICC with PGSI confirmed by postoperative pathological examination. She presented with abdominal pain (50.8 points) and increased serum carcinoembryonic antigen (CEA) level (>5 ng/mL, 100 points). Axial CT image in the portal venous phase shows a non-mass-forming (non-MF) type ICC (43.9 points) with intrahepatic bile duct dilatation (arrow, 69.9 points). Hence, a total score of 264.6 points was obtained, which corresponds to a probability of PGSI >99% according to the lower scale of the nomogram in *Figure 4*. (B) A 60-year-old man of ICC without PGSI confirmed by postoperative pathological examination. He presented with no symptoms (0 points) and normal serum carcinoembryonic antigen (CEA) level (≤5 ng/mL, 0 points). Axial CT image in portal venous phase shows a mass-forming (MF) type ICC (0 points) without intrahepatic bile duct dilatation (0 points). Therefore, a total score of 0 points was obtained, which corresponds to a probability of PGSI around 1% according to the lower scale of the nomogram in *Figure 4*. (C) Histopathological image (HE, ×40) shows an ICC with peritumoral Glisson's sheath invasion in the same patient of (A). Note the tumor cells (arrows) invading peritumoral Glisson's sheath (rectangular box). (D) Histopathological image (HE, ×40) shows an ICC without PGSI in the same patient of (B). No tumor cells can be found in peritumoral Glisson's sheath (rectangular box).

distinct behavior of this malignant tumor preoperatively.

Acknowledgements

Funding: This study has received funding by the Natural Science Foundation of Jiangsu Province (BK20150109), Jiangsu Province Health and Family Planning Commission Youth Scientific Research Project (Q201508), Six Talent Peaks Project of Jiangsu Province (2015-WSN-079), Key Project and outstanding Youth supported by Medical Science and technology development Foundation Nanjing (YKK15067, QRX11178), Jiangsu province key medical young talents, "13th Five-Year" health promotion project of Jiangsu province (QNRC2016041).

Footnote

Conflicts of Interest: The authors have no conflicts of interest to declare.

Ethical Statement: The retrospective study was approved by the local institutional review board, and the informed consent from patients was waived.

References

1. Khan SA, Thomas HC, Davidson BR, Taylor-Robinson SD. Cholangiocarcinoma. Lancet 2005;366:1303-14.
2. Zhao M, Dong L, Liu Z, Yang S, Wu W, Lin J. In vivo fluorescence imaging of hepatocellular carcinoma using a novel GPC3-specific aptamer probe. Quant Imaging Med Surg 2018;8:151-60.
3. Jiang BG, Sun LL, Yu WL, Tang ZH, Zong M, Zhang YJ. Retrospective analysis of histopathologic prognostic factors after hepatectomy for intrahepatic cholangiocarcinoma. Cancer J 2009;15:257-61.
4. Ciresa M, De Gaetano AM, Pompili M, Saviano A, Infante A, Montagna M, Guerra A, Giuga M, Vellone M, Ardito F, De Rose A, Giuliante F, Vecchio FM, Gasbarrini A, Bonomo L. Enhancement patterns of intrahepatic mass-forming cholangiocarcinoma at multiphasic computed tomography and magnetic resonance imaging and correlation with clinicopathologic features. Eur Rev Med Pharmacol Sci 2015;19:2786-97.
5. Sasaki A, Aramaki M, Kawano K, Morii Y, Nakashima K, Yoshida T, Kitano S. Intrahepatic peripheral cholangiocarcinoma: mode of spread and choice of surgical treatment. Br J Surg 1998;85:1206-9.
6. Bosman FT. WHO classification of tumours of the digestive system. 4th ed. Lyon: International Agency for Research on Cancer; 2010.
7. Park HJ, Jang KM, Kang TW, Song KD, Kim SH, Kim YK, Cha DI, Kim J, Goo J. Identification of Imaging Predictors Discriminating Different Primary Liver Tumours in Patients with Chronic Liver Disease on Gadoxetic Acid-enhanced MRI: a Classification Tree Analysis. Eur Radiol 2016;26:3102-11.
8. Tsunematsu S, Chuma M, Kamiyama T, Miyamoto N, Yabusaki S, Hatanaka K, Mitsuhashi T, Kamachi H, Yokoo H, Kakisaka T, Tsuruga Y, Orimo T, Wakayama K, Ito J, Sato F, Terashita K, Nakai M, Tsukuda Y, Sho T, Suda G, Morikawa K, Natsuizaka M, Nakanishi M, Ogawa K, Taketomi A, Matsuno Y, Sakamoto N. Intratumoral artery on contrast-enhanced computed tomography imaging: differentiating intrahepatic cholangiocarcinoma from poorly differentiated hepatocellular carcinoma. Abdom Imaging 2015;40:1492-9.
9. Asayama Y, Yoshimitsu K, Irie H, Tajima T, Nishie A, Hirakawa M, Nakayama T, Kakihara D, Taketomi A, Aishima S, Honda H. Delayed-phase dynamic CT enhancement as a prognostic factor for mass-forming intrahepatic cholangiocarcinoma. Radiology 2006;238:150-5.
10. Yamamoto Y, Türkoğlu MA, Aramaki T, Sugiura T, Okamura Y, Ito T, Ashida R, Uemura S, Miyata T, Kato Y, Kakuta Y, Nakanuma Y, Uesaka K. Vascularity of Intrahepatic Cholangiocarcinoma on Computed Tomography is Predictive of Lymph Node Metastasis. Ann Surg Oncol 2016;23:485-93.
11. Liver Cancer Study Group of Japan. The general rules for the clinical and pathological study of primary liver cancer, 4th, ed. Tokyo: Kanehara and Co. Ltd, 2000:19.
12. Lim JH. Cholangiocarcinoma: morphologic classification according to growth pattern and imaging findings. AJR Am J Roentgenol 2003;181:819-27.
13. He J, Gan W, Liu S, Zhou K, Zhang G, Guo H, et al. Dynamic Computed Tomographic Features of Adult Renal Cell Carcinoma Associated With Xp11.2 Translocation/TFE3 Gene Fusions: Comparison With Clear Cell Renal Cell Carcinoma. J Comput Assist Tomogr 2015;39:730-6.
14. Kim TK, Choi BI, Han JK, Jang HJ, Cho SG, Han MC. Peripheral cholangiocarcinoma of the liver: two-phase spiral CT findings. Radiology 1997;204:539-43.
15. Huh CW, Kim HW, Yi SW, Lee DK, Lee SJ. Common bile duct stones associated with pancreatobiliary reflux and disproportionate bile duct dilatation. Medicine (Baltimore) 2017;96:e7701.
16. Iavarone M, Piscaglia F, Vavassori S, Galassi M, Sangiovanni A, Venerandi L, Forzenigo LV, Golfieri R, Bolondi L, Colombo M. Contrast enhanced CT-scan to diagnose intrahepatic cholangiocarcinoma in patients with cirrhosis. J Hepatol 2013;58:1188-93.
17. Chen J, He J, Deng M, Wu HY, Shi J, Mao L, Sun Q, Tang M, Fan XS, Qiu YD, Huang Q. Clinicopathological, radiologic, and molecular study of 23 combined hepatocellular-cholangiocarcinomas with stem cell features, cholangiolocellular type. Hum Pathol 2017;64:118-27.
18. Weber SM, Ribero D, O'Reilly EM, Kokudo N, Miyazaki M, Pawlik TM. Intrahepatic cholangiocarcinoma: expert consensus statement. HPB (Oxford) 2015;17:669-80.

19. Hur H, Park IY, Sung GY, Lee DS, Kim W, Won JM. Intrahepatic cholangiocarcinoma associated with intrahepatic duct stones. Asian J Surg 2009;32:7-12.
20. Qin XL, Wang ZR, Shi JS, Lu M, Wang L, He QR. Utility of serum CA19-9 in diagnosis of cholangiocarcinoma: in comparison with CEA. World J Gastroenterol 2004;10:427-32.
21. Zheng BH, Yang LX, Sun QM, Fan HK, Duan M, Shi JY, Wang XY, Zhou J, Fan J, Ma ZY, Gao Q. A New Preoperative Prognostic System Combining CRP and CA199 For Patients with Intrahepatic Cholangiocarcinoma. Clin Transl Gastroenterol 2017;8:e118.
22. Si A, Li J, Xiang H, Zhang S, Bai S, Yang P, Zhang X, Xia Y, Wang K, Yan Z, Lau WY, Shi L, Shen F. Actual over 10-year survival after liver resection for patients with intrahepatic cholangiocarcinoma. Oncotarget 2017;8:44521-32.
23. Nakajima T, Kondo Y, Miyazaki M, Okui K. A histopathologic study of 102 cases of intrahepatic cholangiocarcinoma: histologic classification and modes of spreading. Hum Pathol 1988;19:1228-34.
24. Weinbren K, Mutum SS. Pathological aspects of cholangiocarcinoma. J Pathol 1983;139:217-38.
25. Vijgen S, Terris B, Rubbia-Brandt L. Pathology of intrahepatic cholangiocarcinoma. Hepatobiliary Surg Nutr 2017;6:22-34.
26. Valls C, Gumà A, Puig I, Sanchez A, Andía E, Serrano T, Figueras J. Intrahepatic peripheral cholangiocarcinoma: CT evaluation. Abdom Imaging 2000;25:490-6.
27. Lacomis JM, Baron RL, Oliver JR, Nalesnik MA, Federle MP. Cholangiocarcinoma: delayed CT contrast enhancement patterns. Radiology 1997;203:98-104.
28. Sanada Y, Yoshida K, Itoh H. Comparison of CT enhancement patterns and histologic features in hepatocellular carcinoma up to 2 cm: assessment of malignant potential with claudin-10 immunohistochemistry. Oncol Rep 2007;17:1177-82.
29. Nanashima A, Sumida Y, Abo T, Oikawa M, Murakami G, Takeshita H, Fukuoka H, Hidaka S, Nagayasu T, Sakamoto I, Sawai T. Relationship between pattern of tumor enhancement and clinicopathologic characteristics in intrahepatic cholangiocarcinoma. J Surg Oncol 2008;98:535-9.
30. Liu W, Liang W. CT features of hepatic epithelioid angiomyolipoma: differentiation from hepatocellular carcinoma in patients with noncirrhotic livers. Quant Imaging Med Surg 2018;8:597-608.
31. Soyer P, Bluemke DA, Hruban RH, Sitzmann JV, Fishman EK. Intrahepatic cholangiocarcinoma: findings on spiral CT during arterial portography. Eur J Radiol 1994;19:37-42.
32. Maetani Y, Itoh K, Watanabe C, Shibata T, Ametani F, Yamabe H, Konishi J. MR imaging of intrahepatic cholangiocarcinoma with pathologic correlation. AJR Am J Roentgenol 2001;176:1499-507.
33. Zhao YJ, Chen WX, Wu DS, Zhang WY, Zheng LR. Differentiation of mass-forming intrahepatic cholangiocarcinoma from poorly differentiated hepatocellular carcinoma: based on the multivariate analysis of contrast-enhanced computed tomography findings. Abdom Radiol (NY) 2016;41:978-89.

Cite this article as: Mao Y, Zhu Y, Qiu Y, Kong W, Mao L, Zhou Q, Chen J, He J. Predicting peritumoral Glisson's sheath invasion of intrahepatic cholangiocarcinoma with preoperative CT imaging. Quant Imaging Med Surg 2019;9(2):219-229. doi: 10.21037/qims.2018.12.11

